A&A manuscript no.
(will be inserted by hand later)

Your thesaurus codes are:
06 (06.18.1; 02.03.1; 03.13.2; 03.13.6)

ASTRONOMY AND ASTROPHYSICS

February 8, 2008

Determination of fractal dimensions of solar radio bursts

A. Veronig[1], M. Messerotti[2], and A. Hanslmeier[1]

[1] Institute of Astronomy, University of Graz, Universitätsplatz 5, A–8010 Graz, Austria
[2] Trieste Astronomical Observatory, Via G.B. Tiepolo 11, I–34131 Trieste, Italy

Received 19 July 1999 / Accepted 7 March 2000

Abstract. We present a dimension analysis of a set of solar type I storms and type IV events with different kind of fine structures, recorded at the Trieste Astronomical Observatory. The signature of such types of solar radio events is highly structured in time. However, periodicities are rather seldom, and linear mode theory can provide only limited interpretation of the data. Therefore, we performed an analysis based on methods of the nonlinear dynamics theory.

Additionally to the commonly used correlation dimension, we also calculated local pointwise dimensions. This alternative approach is motivated by the fact that astrophysical time series represent real-world systems, which cannot be kept in a controlled state and which are highly interconnected with their surroundings. In such systems pure determinism is rather unlikely to be realized, and therefore a characterization by invariants of the dynamics might probably be inadequate.

In fact, the outcome of the dimension analysis does not give hints for low-dimensional determinism in the data, but we show that, contrary to the correlation dimension method, local dimension estimations can give physical insight into the events even in cases in which pure determinism cannot be established. In particular, in most of the analyzed radio events nonlinearity in the data is detected, and the local dimension analysis provides a basis for a quantitative description of the time series, which can be used to characterize the complexity of the related physical system in a comparative and non-invariant manner.

In this frame, the degree of complexity we inferred for type I storms is on the average lower than that relevant to type IV events. For the type IV events significant differences occur with regard to the various subtypes, whereas pulsations and sudden reductions can be described by distinctly lower values than spikes and fast pulsations.

Key words: Sun: radio radiation – chaos – methods: data analysis – methods: statistical

Send offprint requests to: A. Veronig

1. Introduction

Nonlinear time series analysis based on the theory of deterministic chaos has turned out to be a powerful tool in understanding complex dynamics from measurements and observational time series. In particular it can provide descriptions and interpretations for irregular times series, which nevertheless might not be governed by a stochastic physical process and which are only poorly understood by linear methods. A number of recent reviews and conference proceedings shows the great interest in the field of nonlinear time series analysis (see, for instance, Grassberger et al. 1991; Casdagli & Eubank 1992; Weigend & Gershenfeld 1993; Kugiumtzis 1994a, 1994b; Abarbanel 1996; Kantz & Schreiber 1997; Schreiber 1999).

Since the development of chaos theory, it is well known that even simple dynamical systems, described by few nonlinear differential equations, can reveal a complex and quasi-irregular behavior. A central concept to characterize such systems is the so-called *attractor*. Under the dynamics of a deterministic system the trajectories do not cover the whole phase space, but, after all transient phenomena have faded out, converge to a subset of the phase space, the attractor. The attractor itself is invariant to the dynamical evolution. Simple examples of attractors are fixed points and limit cycles. However, when the related dynamical system is *chaotic*, the attractor can have a complex geometry with a *fractal*, i.e., non-integer, dimension. Different invariant parameters exist to describe the geometry and the dynamics of an attractor, such as dimensions, Lyapunov exponents and entropies. Besides the fractal geometry, chaotic systems have the striking property that initially neighboring trajectories diverge exponentially under the dynamics, and the growth rate is given by the *Lyapunov exponent*. This phenomenon results from the folding and stretching of the trajectories under the dynamics, the folding leading to the convergence of the trajectories to the attractor and the stretching to the divergence in certain directions. While the average stretching rate is given by the Lyapunov exponent, the loss of information due to the folding is quantified by the *entropy*. Lyapunov exponents and entropies characterize the dynamics on the attractor,

and the *dimension* characterizes its geometry. The physical meaning of the dimension of an attractor is that it corresponds to the degree of freedom of the related dynamical system, i.e., in a deterministic case, the minimum number of ordinary differential equations needed to fully describe the system. Deterministic systems are characterized by a finite dimension. Deterministic chaotic systems have the additional characteristic that their dimension is fractal. Contrary to that, a stochastic system is characterized by an infinite dimension, indicating its infinite degree of freedom. Therefore, the determination of the dimension of an attractor enables to discriminate whether a dynamical system is deterministic or stochastic.

Previous papers exist concerning the investigation of fractal dimensions of solar radio bursts. It has to be noted, that the time series used by the different authors are not directly comparable as they represent different types of radio events. Kurths & Herzel (1986, 1987), Kurths & Karlický (1989), and Kurths et al. (1991) analyzed decimetric pulsations and ascertained finite dimension values. Contrary to that, Isliker (1992b) and Isliker & Benz (1994a, 1994b) investigated different types of solar radio bursts in the metric (m) and decimetric (dm) wavelength range (type I storms, type II bursts, type III bursts, type IV events, and narrowband spikes), which did not reveal any hints for low-dimensional determinism.[1]

However, these investigations rely all on the correlation dimension method. The present paper additionally introduces a complementary dimension analysis, motivated by the fact that solar radio bursts represent real-world systems, which implies some major restrictions. First, the time series cannot be expected to be stationary, and second, pure determinism is rather unlikely to be realized. Therefore we do not only concentrate on the usual way of looking at the problem: "Does the analyzed time series represent a deterministic or a stochastic system?" but in particular focus the question: "What statistical description can be extracted from a dimension analysis of the time series?" With such refined formulation of the problem, we try to make use of the concepts and tools of nonlinear time series analysis even in cases in which the determination of invariants of the dynamics, as, e.g., attractor dimensions, possibly fails.

The paper is structured as follows. Sect. 2 explains the used methods and discusses critical points in the determination of fractal dimensions from time series. In Sect. 3 the investigated data sets are characterized and the analysis procedure is described. Sect. 4 presents the results of the dimension analysis, which are discussed in Sect. 5. Finally, the conclusions are drawn in Sect. 6.

2. Methods

[1] The reported finite dimension for one of the analyzed narrowband spike events in Isliker (1992b) was revised in a later paper (Isliker & Benz 1994a).

2.1. Phase space reconstruction

Generally, not all relevant parameters of the dynamics of a system are measured during an observation but only a one-dimensional time series is given. To reconstruct the phase space of the related dynamical system, techniques have to be applied to unfold the multi-dimensional attractor from a scalar time series. By the technique of time delayed coordinates (Takens 1981), from a given one-dimensional time series $\{x(t_i)\}$ an m-dimensional phase space $\{\boldsymbol{\xi}_i\}$ is built up by the prescription

$$\boldsymbol{\xi}_i = \{x(t_i),\ x(t_i+\tau),\ \ldots\ , x(t_i+(m-1)\tau)\}\ , \qquad (1)$$

where τ is the time delay.

According to the embedding theorem of Takens (1981), the embedding of the attractor in the m-dimensional reconstructed phase space can be ensured if $m \geq (2D+1)$, with D the dimension of the original phase space. For time series of infinite length and accuracy, τ can be chosen in a more or less arbitrary way without affecting the results. However, in practice not every value for the time delay τ will be suitable. Too small τ will build up coordinates which are too strongly correlated, while for large τ the vector components show no causal connection. The choice of the time delay τ in the reconstruction of the phase space usually strongly affects the quality of the analysis, and different procedures have been worked out to ensure a proper choice of τ. The most prominent methods use the auto-correlation time ($1/e$ decay time, first zero crossing, first minimum) or the first minimum of the mutual information (Fraser & Swinney 1986).

One advantage of the *mutual information* over the auto-correlation function is that it takes into account nonlinear properties of the data. The mutual information is based on the Shannon entropy (Shannon & Weaver 1962), and gives the information about the state of a system at time $t+\tau$ that we already possess if we know the state at time t. The choice of the first minimum of the mutual information for the time delay τ is motivated by the fact that two successive delay coordinates should be as independent as possible without making τ too large.

2.2. Correlation dimension

The correlation dimension is one out of many definitions of fractal dimensions, and was introduced by Grassberger & Procaccia (1983a, 1983b) to determine fractal dimensions from time series. The correlation dimension is based on distance measurements of points in phase space. Therefore, as first step, from the time series $\{x(t_i)\}$ the phase space vectors $\{\boldsymbol{\xi}_i\}$ have to be constructed. With the reconstructed vectors, the correlation integral $C(r)$ can be calculated, which is given by the normalized number of pairs of points within a distance r. As the correlation dimension is based on spatial correlations in phase space, it is an important precaution to exclude serially correlated

points in counting the pairs (for details see Sect. 2.4.2), and the length of the window, W, should at least cover all points within the auto-correlation time (Theiler 1986). With this correction, the correlation integral is given by

$$C(r) = \frac{2}{\mathrm{N_{pairs}}} \sum_{i=1}^{\mathrm{N}-W} \sum_{j=i+W}^{\mathrm{N}} \Theta(r - \|\boldsymbol{\xi}_i - \boldsymbol{\xi}_j\|)\,, \tag{2}$$

$$\mathrm{N_{pairs}} = (\mathrm{N} - W)(\mathrm{N} - W + 1)\,, \tag{3}$$

where N denotes the overall number of data points, and Θ is the Heaviside step function. For small distances r, the correlation integral $C(r)$ is expected to scale with a power of r, and the scaling exponent defines the correlation dimension D_c:

$$C(r) \propto r^{D_c}\,, \quad \text{for } r \to 0\,, \tag{4}$$

$$D_c = \lim_{r\to 0} \frac{\ln C(r)}{\ln r}\,. \tag{5}$$

Practically one computes the correlation integral for increasing embedding dimension m and calculates the related $D_c(m)$ in the scaling region. If the $D_c(m)$ reach a saturation value D_c for relatively small m, this gives an indication that an attractor with dimension D_c exists underlying the analyzed time series.

2.3. Local pointwise dimensions

The local pointwise dimension is a locally defined variant of the correlation dimension. Its definition is based on the probability $p_i(r)$ to find points in a neighborhood of a point $\boldsymbol{\xi}_i$ with size r:

$$p_i(r) = \frac{1}{\mathrm{N_{pairs}}} \sum_{\substack{j=1 \\ |j-i|\geq W}}^{\mathrm{N}} \Theta(r - \|\boldsymbol{\xi}_i - \boldsymbol{\xi}_j\|)\,, \tag{6}$$

where $\mathrm{N_{pairs}}$ gives the actual number of pairs of points in the sum. For small distances r, $p_i(r)$ is expected to scale with a power of r, and the scaling exponent $D_p(\boldsymbol{\xi}_i)$ gives the local pointwise dimension at point $\boldsymbol{\xi}_i$:

$$p_i(r) \propto r^{D_p(\boldsymbol{\xi}_i)}\,, \quad \text{for } r \to 0\,, \tag{7}$$

$$D_p(\boldsymbol{\xi}_i) = \lim_{r\to 0} \frac{\ln p_i(r)}{\ln r}\,. \tag{8}$$

Averaging $D_p(\boldsymbol{\xi}_i)$ over all points of the time series or a number of reference points yields the averaged pointwise dimension, $\bar{D}_p$, which is equivalent to the correlation dimension and gives a global description of the geometry of an attractor:

$$\bar{D}_p = \frac{1}{\mathrm{N_{ok}}} \sum_{i=1}^{\mathrm{N_{ok}}} D_p(\boldsymbol{\xi}_i)\,, \tag{9}$$

with $\mathrm{N_{ok}}$ the number of accepted reference points.

Since the $D_p(\boldsymbol{\xi}_i)$ are local functions and defined for each point, they are, on the one hand, a function of the position $\boldsymbol{\xi}_i$ on the attractor, characterizing its local geometry. On the other hand, the local dimensions can be interpreted as a function of time, $D_p(t_i)$, since they reflect the temporal evolution, in which the points $\boldsymbol{\xi}_i$ on the attractor are covered by the dynamics (Mayer-Kress 1994). Based on this fact, local dimension estimations have the interesting property that they enable to cope with non-stationary data.

An example is shown in Fig. 1, which illustrates the local pointwise dimensions calculated for a simulated time series, made up of three sections related to different attractors, the Lorenz, a limit cycle and the Rössler attractor. The evolution of the local pointwise dimensions $D_p(t_i)$ detects the different attractors successively operating in time. The averaged pointwise dimensions $\bar{D}_p$ in the respective sections deviate less than 10% from the true values. As for the calculation of the local dimension at point $\boldsymbol{\xi}_i$ the distances to *all* points of the time series, even those related to a different attractor, are taken into account, it is a quite striking feature that the different attractors can be disentangled by the method. Moreover, for this exemplary analysis the length of the time series was taken rather short in order to mimic the conditions of observed time series. Such a behavior reveals that the reference point $\boldsymbol{\xi}_i$, which is equivalent to a time t_i of the dynamical evolution of the system, dominates the local dimension calculation. However, we want to stress that small changes of the attractor dimension, as, e.g., in the case of the Lorenz and the Rössler attractor (see Fig. 1), cannot be detected .

2.4. Pitfalls in dimension estimations

The determination of fractal dimensions from time series, characterized by finite length and accuracy, includes many pitfalls, which can lead to quite spurious results. In this chapter the most prominent problems will be discussed and the strategies used by the authors to avoid such pitfalls. A brief but quite dense review with respect to critical points in the determination of the correlation dimension can be found in Grassberger et al. (1991). As the local pointwise dimensions are a variant of the correlation dimension, most of the problems occur in a similar way.

2.4.1. Noise and quality of the scaling region

As expressed in Eq. 4 for the correlation integral $C(r)$ and Eq. 7 for the probability $p_i(r)$, respectively, a scaling behavior is expected for $r \to 0$. However, for real time series, which are contaminated by noise and which are of finite length, the scaling behavior is expected to occur at intermediate length scales. Noise is acting at small scales and therefore dominating the scaling behavior for small r. Deviations from ideal scaling at large length scales are

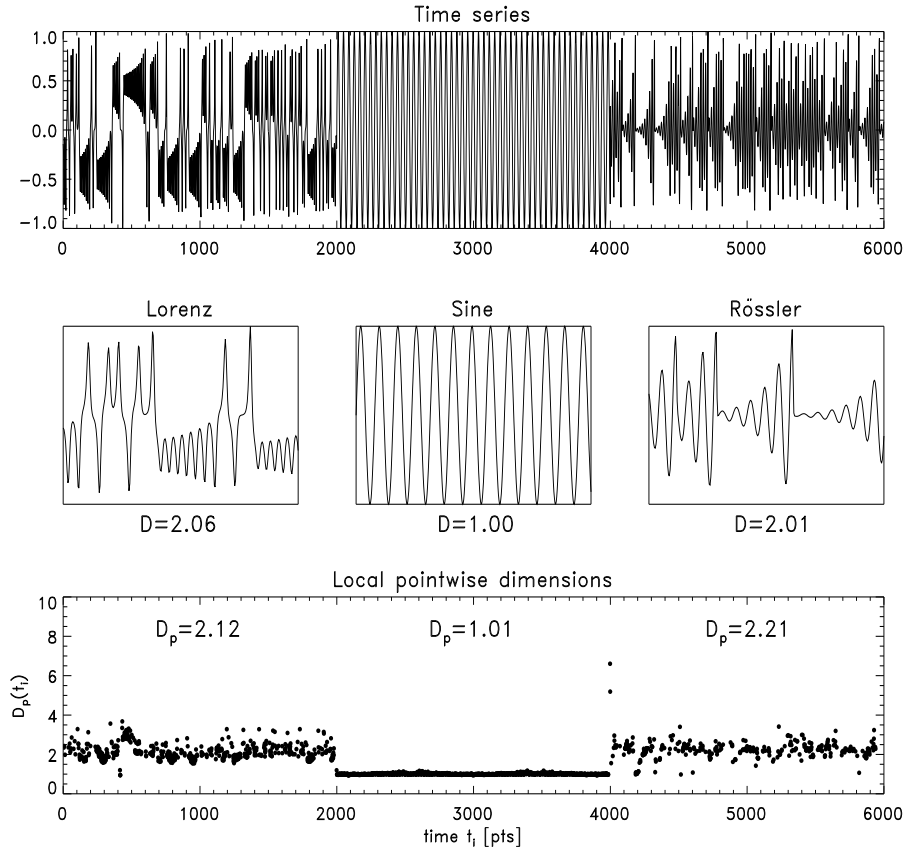

Fig. 1. Top Panel: Simulated time series, made up of three sections related to different attractors, the Lorenz, a limit cycle (Sine), and the Rössler attractor. The middle panels depict an enlargement of the respective sections. The bottom panel shows the related local pointwise dimensions $D_p(t_i)$. Its evolution reflects the different attractors successively operating in time.

due to edge effects caused by the finite length of the time series.

Fig. 2 shows such typical scaling behavior for a time series of finite length and accuracy. For better illustration we have plotted the local slopes of the correlation integral, given by the expression

$$\nu(r) = \frac{\mathrm{d}\ln C(r)}{\mathrm{d}\ln r}\,. \tag{10}$$

In the case of ideal scaling, the $\nu(r)$, calculated for different embedding dimensions m, form straight lines parallel to the x-axes, the so-called plateau region, with the constant y-value corresponding to $D_c(m)$. However, it is typical for observational time series that at least three different parts in the $\nu(r)$ curves are distinguishable, described in the caption of Fig. 2. To avoid spurious finite dimensions which might arise from a misinterpretation of the existence or non-existence of a physically relevant scaling region, we implemented an algorithm to automatically check for scaling behavior (see Sect. 2.5).

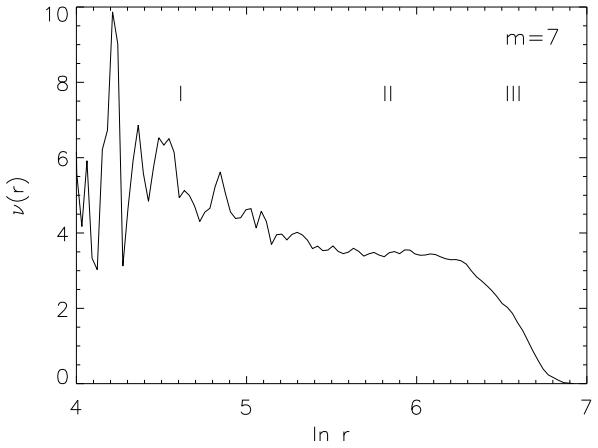

Fig. 2. Scaling behavior for a time series of finite length and accuracy, calculated from a stationary subsection of a type IV event with sudden reductions (January 13, 1989). On small scales r [I], the scaling is dominated by noise. Since noise tends to fill the whole phase space: $\nu(r, m) \approx m$. At intermediate length scales [II], the physically relevant scaling is located: $\nu(r, m) \approx D_c(m)$. For large r [III], deviations from the ideal scaling occur due to the finite number of data points.

2.4.2. Temporal correlations

The correlation integral $C(r)$ and the probability $p_i(r)$ are a measure of spatial correlations on the attractor. They are basically calculated by counting pairs of points which are closer to each other than a given distance r. However, at small scales successive points of the time series give an additional contribution, since they are close in time. Nevertheless, such points do not reflect spatial correla-

tions, i.e., a clustering of points in phase space, but are serially correlated by the temporal order of the time series. To avoid the spurious contribution of serially correlated points, which can cause strong artificial effects, especially for data recorded with a high sampling rate, at least all pairs of points closer than the auto-correlation time have to be excluded (Theiler 1986):

$$W > t_{corr}\,. \tag{11}$$

A similar phenomenon can occur when the analyzed time series is rather short. If the time series is too short to ensure that the attractor is well covered with points, then most of the points of the series are serially correlated, which again might result in spurious dimensions. Different relations have been derived for the minimum length of a time series needed for dimension estimations, as the one by Eckmann & Ruelle (1992):

$$D_c < 2\log_{10}\mathrm{N}\,, \tag{12}$$

with N the length of the time series. However, not only the length of the data series is of relevance but also the length with regard to the sampling rate. Applications to different kind of time series, from known chaotic attractors as well as measured time series (Brandstater & Swinney 1987; Kurths et al. 1991; Isliker 1992a; Isliker & Benz 1994a), have revealed that the analyzed time series should at least cover 50 structures – "structure" meaning a full orbit in phase space or generally a typical time scale of the analyzed time series. According to Isliker (1992a), we define the structures by the first minimum of the auto-correlation function,

$$\mathrm{N}_{str} \gtrsim 50 \quad \text{with} \quad \mathrm{N}_{str} := \frac{\mathrm{N}\cdot\Delta}{t_{corr}}\,, \tag{13}$$

where N_{str} gives the number of structures, N the length of the time series, Δ the temporal resolution, and t_{corr} the auto-correlation time.

2.4.3. Stationarity

As shown by Osborne et al. (1986) and Osborne & Provenzale (1989), the determination of the correlation dimension from non-stationary stochastic processes, can erroneously lead to finite dimension values. To take into account that problem, we applied a stationarity test proposed by Isliker & Kurths (1993), which is based on the binned probability distribution of the data. To check for stationarity one divides the time series into subsections, and compares the probability distribution of the section under investigation with the probability distribution of the first half of it by a χ^2-test. By the use of this test we searched for stationary subsections in the radio burst time series, and only to such stationary subsections the correlation dimension analysis was applied.

However, with the concept of local dimensions it is possible to cope with non-stationary data. One important advantage of the local dimension method is that it can enable to detect dynamical changes in a time series. To make use of this potentiality, we calculated the local pointwise dimensions from the whole time series instead of using stationary subsections. Moreover, since the statistics in the calculation of the local pointwise dimensions grows linearly with the length of the time series, whereas the correlation dimension grows with the square of the number of points, for the local pointwise dimension analysis the time series should be kept as long as possible. However, to avoid spurious results due to non-stationarities, we applied a surrogate data test (Sect. 2.6).

2.4.4. Intermittency

Intermittency describes the phenomenon that a time series is interrupted by quiet phases or phases of very low amplitudes. Such a phenomenon is quite typical for chaotic systems, but can cause problematic situations when calculating fractal dimensions from limited time series. In phase space the intermittent sections represent regions, which, in the context of the global attractor scale, degenerate to a point. This would trivially result in an erroneously low dimension value. One way to cope with this problem is just to discard intermittent phases from the analyzed time series. Since the dimension of an attractor is a geometric descriptor, which means a static quantity, it is not influenced by the serial order of points, and therefore discarding subsections is a valid strategy.

As an example, the top panel of Fig. 3 shows the subsection of a type I burst series. The middle and bottom panels show the results of the correlation dimension analysis, calculated from the whole time series (middle panels) and the time series after the intermittent section was eliminated (bottom panels). A comparison of the middle and bottom panels reveals that the intermittent phase causes a deformation in the curves of the correlation integral and the related local slopes. Eliminating the intermittent section, these deformations disappear. However, we want to stress that the used algorithm for the automatic detection of the scaling region does not identify the sink-region as a scaling region, which could result in spurious finite dimensions. Therefore, by the set up of the scaling algorithm we avoid erroneous low dimensions caused by intermittency effects.

2.5. Scaling and convergence test

The practical computation of the local pointwise dimensions turns out to be more difficult than the correlation dimension, particularly as for *each* reference point the scaling region has to be determined and the related $D_p(\boldsymbol{\xi}_i, m)$, which are calculated in the scaling region, have to be checked for convergence with increasing embedding dimension m. For this purpose, an automatic and fast procedure is needed. Moreover, such an automatic procedure

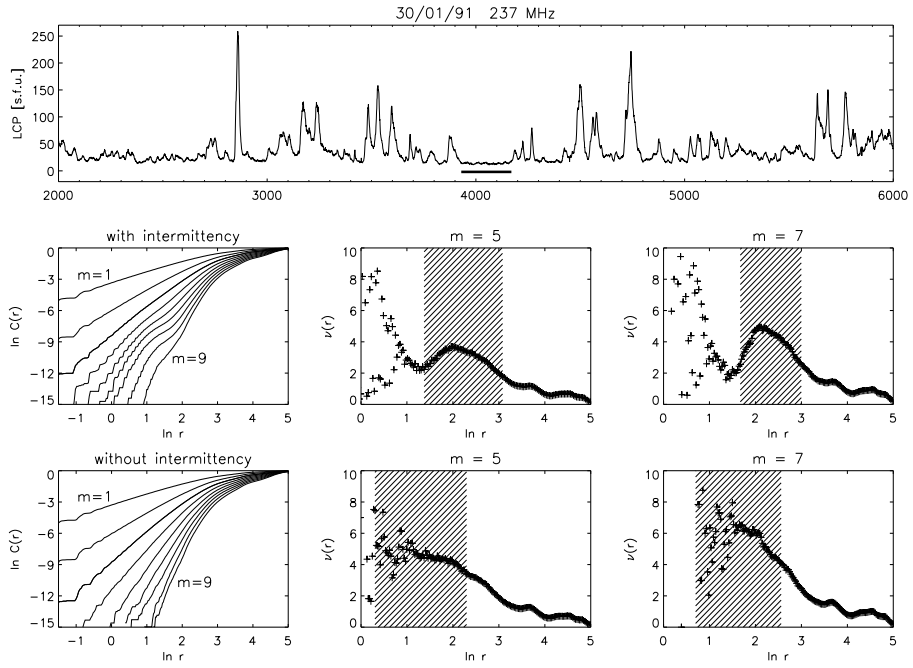

Fig. 3. Top panel: Stationary subsection of a type I storm (January 30, 1991) with an intermittent phase present (marked by a line). The abscissa values are given in points (the same applies to following figures). Middle panel: Correlation integral $C(r)$ for $m = 1$ to $m = 9$, and local slopes $\nu(r)$ for $m = 5$ and $m = 7$, calculated from the whole time series depicted. Bottom panels: Same curves, but calculated from the time series after the putative intermittent section was eliminated. The hatched ranges in the graphs of the local slopes mark the automatically determined scaling region.

can also be used in the correlation dimension analysis to avoid subjective influences on the scaling and convergence judgement. We implemented such an algorithm, based on the one used by Skinner et al. (1991), but modified in order to reach higher stability and significance. This automatic procedure searches for the scaling region, defined as the longest linear range in the $\ln p_i(r)$ curves, tests if the scaling region is of significant length, and finally checks if the $D_p(\boldsymbol{\xi}_i, m)$ are converging with increasing m. Only for points $\boldsymbol{\xi}_i$, which pass the scaling and the convergence test, a local pointwise dimension $D_p(\boldsymbol{\xi}_i)$ is accepted. In the following we give a description of the algorithm.

According to Eq. 6, for each reference point $\boldsymbol{\xi}_i$ and each considered embedding dimension m, we calculate the cumulative histogram of the $p_i(r)$, dividing the r-range into 100 equidistant points in the logarithmic representation, which cover the whole range from the smallest to the largest actual distance. The local slopes of the $\ln p_i(r)$ versus $\ln(r)$ curves, given by

$$\nu_i(r) = \frac{\mathrm{d} \ln p_i(r)}{\mathrm{d} \ln r}\,, \tag{14}$$

calculated in the scaling region, represent the $D_p(\boldsymbol{\xi}_i, m)$. For the determination of the location of the scaling range, we shift a window with length 10 points through the overall r-range, and for each of these windows a least squares linear fit is applied to the $\ln p_i(r)$ versus $\ln r$ curves. The slope of the linear fit corresponds to the average value of the local slopes in the corresponding r-range, denoted as $\bar{\nu}_i(r)$. Starting with the first window, successive $\bar{\nu}_i(r)$ are compared with the corresponding quantity in the first window, until the difference is larger than a certain threshold value, chosen as 20% of the initial $\bar{\nu}_i(r)$. In this case, the position of the first point of the start window and the last point of the actual window are stored, and the procedure continues with the second window as start window. If the new positions determined cover a larger range than the old ones, the old values are overwritten by the new ones, and so on. The two stored values remaining at the end give the location of the scaling region, in which we calculate $D_p(\boldsymbol{\xi}_i, m)$. If the determined scaling region is smaller than 20% of the overall length, it is interpreted as not significant and rejected. To avoid spurious results at large r, which usually correspond to small $\bar{\nu}_i(r)$ values, in the whole procedure we suppress values $\bar{\nu}_i(r) < 2$. Fig. 4 shows a sample application of the algorithm detecting the scaling range.

After the scaling region is determined for each point $\boldsymbol{\xi}_i$ and each embedding dimension m, for those points which reveal a scaling region of significant length for all considered m-values, we test the convergence of the $D_p(\boldsymbol{\xi}_i, m)$ with increasing m. This is simply done by averaging the $D_p(\boldsymbol{\xi}_i, m)$ over four successive m-values. If the standard deviation turns out to be less than 15% of the average value, the convergence is accepted, and the average of the $D_p(\boldsymbol{\xi}_i, m)$ over the considered m-range is taken as local pointwise dimension $D_p(\boldsymbol{\xi}_i)$. The different kind of threshold values used have been adjusted by application of the algorithm to different time series, and slight changes do not qualitatively change the outcome.

2.6. Surrogate data test

As already mentioned, local dimensions enable to deal with non-stationary data. However, to avoid spurious dimensions which can result from non-stationary stochastic processes, we applied a surrogate data test (Osborne et

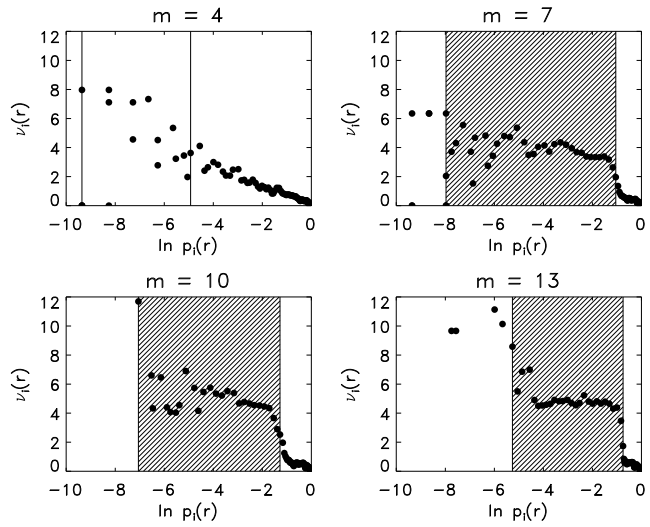

Fig. 4. The curves of local slopes $\nu_i(r)$, with $i = 1300$, are shown for different embedding dimensions m, calculated from a sample type I storm (August 21, 1991). For better illustration we plot $\nu_i(r)$ versus $\ln p_i(r)$ instead of $\nu_i(r)$ versus $\ln r$. The marked regions indicate the location of the scaling range, as detected by the automatic procedure. For $m = 4$ the determined scaling region is too short (less than 20% of the overall r-range), and therefore rejected.

al. 1986; Theiler et al. 1992). For this purpose, a Fourier transform of the time series is performed, the Fourier phases are randomized, and finally to this phase-altered series the inverse Fourier tranform is applied. The phase randomization keeps the power spectrum unchanged while linear correlations in the time series are eliminated. If the results of the dimension analysis of such an ensemble of surrogate data are significantly different from those computed from the original data, the hypothesis can be rejected that the obtained results are caused by a linear stochastic process, and nonlinearity in the data is detected.

To quantify the statistical significance we make use of a hypothesis testing given in Theiler et al. (1992). The null hypothesis assumes that the original data represent linearly correlated noise. To compute a discrimination statistics we need a set of surrogate data, from which the same statistical quantities are derived as from the original time series. In particular, we use the averaged pointwise dimensions as function of the embedding dimension, $\bar{D}_p(m)$. Let Q_o denote the statistical quantity computed for the original time series, and Q_{s_i} for the ith surrogate generated under the null hypothesis. Let μ_s and σ_s represent the (sample) mean and standard deviation of the distribution of Q_s. With this notation the measure of "significance", S, is given by the expression

$$S = \frac{|Q_o - \mu_s|}{\sigma_s} \,. \tag{15}$$

3. Data sets and analysis procedure

The data sets are single frequency recordings from the multichannel radio-polarimeter of the Trieste Astronomical Observatory, which is operating in the dm-m wavelength range. The investigated data sets are recorded at the frequencies 237, 327, 408 and 610 MHz, with a sampling rate of 50 Hz, i.e. a temporal resolution $\Delta = 20$ ms. We analyzed 30 data sets of type I storms and 27 sets of type IV events, which cover samples with different kind of fine structures, such as pulsations, fast pulsations, sudden reductions and spikes. Some of the events were analyzed at different times and/or frequencies. Therefore, the 30 data sets of type I storms represent 24 different events, the 27 data sets of type IV events 20 different ones. In Table 1 and Table 2 we give a description of the type I and type IV events, respectively. The main criteria for the data selection from the solar radio burst data archive of the Trieste Observatory were:

1. The selected data sets were representative for the particular types of events.
2. To ensure a high signal-to-noise ratio only intense events were selected.
3. The related time series were substantially long and fulfilled Eq. 13.

For the analysis, the predominant polarization sense, LCP (Left-handed Circular Polarization) or RCP (Right-handed Circular Polarization) of the burst series was used.

The first step in the correlation dimension analysis was to search for stationary subsections by shifting windows with decreasing length through the time series and applying the stationarity test proposed by Isliker & Kurths (1993). Only those stationary subsections which still fulfilled the minimum length criterion of Eq. 13 were accepted for further analysis, and the correlation dimension was calculated only from such subsections. The analysis was repeated with different values for the delay parameter τ, located around the first minimum of the mutual information. The relevant quantities were calculated up to embedding dimension $m = 20$. Finally, the algorithm for automatically searching the scaling region, checking its validity and testing the convergence behavior was applied. The convergence was checked for m-intervals containing four successive embedding dimensions, starting with $m = 10$.

The pointwise dimension analysis was basically carried out in the same manner, except that the overall time series was used instead of stationary subsections. Moreover, only for points which passed both scaling and convergence test a local pointwise dimension was accepted. Finally, the pointwise dimension analysis was repeated for 10 different sets of surrogate data to test against the null hypothesis that the results are caused by linearly correlated noise, and to get evidence on nonlinearity in the data.

Table 1. Summary of the analyzed type I storms. The first set of columns gives a description of the events, including the date and start time in UT, the available number of data points, the recording frequency in MHz, and the predominant polarization sense (L for Left, R for Right handed circular polarization). Each event was recorded with a temporal resolution of 20 ms. In the second set of columns, for each event the longest stationary subsection (given in number of points) is listed. The third set contains the results of the pointwise dimension analysis. We list the mutual information t_{mut} in points, the averaged pointwise dimension $\bar{D}_p$ with standard deviation σ, the percentage of points passing the scaling and convergence test ("ok"), the increase of the averaged pointwise dimension with increasing embedding dimension in percent, $\Delta\bar{D}_p$, and the outcome of the surrogate data test (pos(itive) means that the null hypothesis can be rejected and nonlinearity is detected).

Date	Start [UT]	Dur. [pts]	Frequ. [MHz]	Pol.	Stat. sect. [pts] from	to	t_{mut} [pts]	$\bar{D}_p$ [dim]	σ [dim]	ok [%]	$\Delta\bar{D}_p$ [%]	surr.
29/04/84	11:06:00	6000	237	L	0	3600	13	5.3	1.3	55	7.2	pos.
	14:50:30	4000	237	L	200	2800	14	5.6	2.0	43	5.1	neg.
	14:54:40	10000	237	L	200	7800	21	6.2	1.5	50	4.1	pos.
25/11/84	13:58:55	1750	237	R	550	1750	5	5.1	1.3	55	8.8	neg.
14/05/85	11:34:00	12000	237	R	0	4000	17	6.4	1.6	42	6.8	pos.
16/05/85	12:51:20	8000	237	R	400	5400	13	6.3	1.3	52	7.7	pos.
06/04/89	06:42:00	6000	237	L	0	3000	9	5.1	1.3	45	5.6	neg.
07/04/89	11:26:05	3000	327	L	0	2800	10	4.9	1.4	51	5.9	pos.
03/05/89	13:33:00	5500	237	L	2400	5500	12	5.3	1.6	47	4.9	neg.
23/06/89	10:13:30	4500	237	R	400	4000	13	5.3	1.4	48	6.5	pos.
14/07/89	08:48:00	3500	237	L	0	3200	14	5.2	1.3	55	4.8	pos.
19/10/89	08:30:20	3500	237	L	0	2000	6	5.4	1.5	55	7.0	pos.
23/11/89	12:17:00	9000	237	R	400	8400	22	6.1	1.4	42	5.5	pos.
	12:12:20	7000	327	R	400	4000	14	6.2	1.3	54	5.9	pos.
04/01/90	11:23:20	11000	237	R	0	7800	16	6.0	1.3	50	5.3	pos.
06/01/90	09:04:40	3500	327	R	200	3400	8	5.0	1.1	52	4.6	pos.
01/03/90	15:03:40	5000	237	L	1000	4000	18	5.6	1.3	51	5.0	pos.
24/07/90	12:42:00	12000	237	R	2000	9000	21	5.7	1.1	50	5.0	pos.
	13:13:00	5500	237	R	0	2200	10	5.5	1.3	52	7.0	pos.
22/11/90	11:37:10	5000	237	L	0	2000	12	5.9	1.4	49	5.3	pos.
29/01/91	12:36:00	6000	237	L	1200	6000	19	5.9	1.6	46	7.7	neg.
30/01/91	12:04:20	7000	237	L	600	5600	23	5.9	1.4	47	5.3	pos.
08/05/91	10:11:30	3000	327	R	1200	2200	8	5.3	1.4	48	4.7	pos.
10/05/91	09:57:30	3500	327	R	60	2340	9	4.9	1.1	51	4.6	neg.
	14:16:00	8000	327	R	1000	7000	14	5.8	1.6	43	4.3	neg.
11/05/91	10:34:00	5000	237	R	600	2500	9	5.1	1.4	38	4.9	pos.
	11:00:20	11000	237	R	1000	10600	18	5.6	1.4	49	5.3	pos.
21/08/91	07:54:00	12000	237	R	3000	12000	17	5.7	1.5	50	4.9	pos.
23/08/91	10:47:20	7000	408	R	200	7000	14	5.7	1.6	50	4.9	pos.
28/01/92	09:27:20	3000	408	R	200	3000	10	5.7	1.3	47	3.6	pos.

4. Results

4.1. Correlation dimension analysis

The application of the stationarity test led to the result, that only two of the preselected events did not reveal stationary subsections fulfilling Eq. 13. These events were excluded from further analysis. For each of the other events, the longest stationary subsections analyzed are listed in Table 1 and Table 2. If more stationary subsections were found, for the analysis the longest three were selected, and non overlapping or only partially overlapping subsections were preferred. The correlation dimension analysis of the stationary subsections did not reveal a finite dimension for any of the events. We identify mainly three cases, in which negative results occurred: *no convergence*, *no scaling region*, and *deformed scaling region*. These three cases are of course ideal ones, and the practice quite often revealed a mixture of it. Therefore, for the single event sections analyzed, we do not specify the different reasons causing the negative result, but describe and discuss the principal cases in the following subsections in a general frame.

4.1.1. No convergence

If the $D_c(m)$ converge with increasing embedding dimension m, this gives indications for the existence of a low-dimensional attractor underlying a time series. In the analyzed data sets, for which the $C(r)$ curves revealed a clear scaling region, no convergence with increasing m occurred. As an example, Fig. 5 shows the divergent behavior for a

Table 2. Summary of the analyzed type IV events. The same quantities as in Table 1 are listed. Additionally, if particular fine structures are present in an event, the predominant type of fine structure is listed (pulsations, fast pulsations, sudden reductions, and spikes).

Date	Start [UT]	Dur. [pts]	Frequ. [MHz]	Pol.	fine str.	Stat. sect. [pts] from	to	t_{mut} [pts]	$\bar{D}_p$ [dim]	σ [dim]	ok [%]	$\Delta\bar{D}_p$ [%]	surr.
10/02/84	14:44:00	4500	237	L		1820	4300	14	6.1	1.2	40	7.1	pos.
14/07/84	09:25:00	6000	237	R		3000	5400	12	5.8	1.4	48	5.1	pos.
24/04/85	10:32:00	12000	237	R	fast puls.	3000	10000	9	7.9	1.4	53	7.4	neg.
07/02/86	10:50:40	10000	408	L	spikes,	1000	9000	8	7.0	1.3	46	6.4	pos.
02/01/89	10:19:00	3000	408	R	sudd. red.	1050	2750	7	5.1	2.1	45	4.9	pos.
13/01/89	12:33:00	8000	408	L	sudd. red.	200	2400	10	5.9	2.2	54	1.1	pos.
12/03/89	07:35:50	6000	327	L	puls.	200	6000	9	6.2	1.4	45	6.3	pos.
30/11/89	12:09:20	2000	610	L	spikes	200	1400	4	6.3	2.6	27	5.4	pos.
19/10/89	12:54:30	4500	610	R		1000	4400	10	6.4	1.9	45	6.8	pos.
	12:58:20	4500	408	R		2320	3200	13	5.3	1.4	50	5.2	pos.
19/12/89	10:34:10	1500	610	L	spikes	200	1400	4	5.6	2.4	40	4.7	pos.
27/12/89	13:44:05	2000	408	R	puls.	200	2000	5	7.0	1.4	46	5.6	neg.
	13:47:40	3500	610	R	sudd. red.	2450	3200	3	5.6	1.8	48	4.8	pos.
17/04/90	14:30:10	1250	610	R		100	1050	4	6.0	1.3	41	6.8	pos.
15/05/90	13:16:50	4000	408	L	spikes	0	750	6	6.1	1.7	56	7.2	pos.
02/07/90	09:42:00	10000	237	L		1000	10000	21	7.0	1.6	38	5.7	neg.
27/11/90	11:05:30	6000	327	R	puls.	2000	6000	9	4.6	1.3	45	3.0	pos.
07/03/91	08:31:20	3500	327	L	puls.	0	3200	12	4.8	1.3	60	9.1	pos.
10/07/91	12:05:20	3000	237	R	puls.	0	2400	12	5.7	1.8	40	6.6	pos.
	12:04:40	10000	327	R	fast puls.	4000	8000	7	7.0	1.5	35	3.2	pos.
	12:04:00	12000	408	R	fast puls.	1000	5000	8	8.2	1.3	54	8.4	pos.
	12:04:00	12000	610	L	fast puls.	5000	10000	6	7.8	1.5	48	7.9	neg.
	12:08:00	6000	610	L	fast puls.	1200	4800	5	7.1	1.6	47	4.7	pos.
22/07/91	09:48:00	6000	610	R	puls.	1200	3800	10	6.1	1.4	37	4.1	pos.
11/11/91	12:42:30	4500	610	L		200	4400	8	6.0	1.5	52	7.4	pos.
27/02/92	11:45:40	6000	237	L	fast puls.	1500	3050	7	7.1	1.7	49	6.4	pos.
	11:56:40	10000	237	L	fast puls.	0	6000	4	7.6	1.2	59	8.4	pos.

type IV event. Even for rather high embedding dimensions a distinct scaling region exists. However, as the curves of the local slopes $\nu(r)$ clearly reveal, the plateau of the scaling region moves to higher values for increasing m, indicating that the $D_c(m)$ are divergent. The meaning of such a divergent behavior can be manifold, being related to the physical state of the system as well as to restrictions regarding the analysis methodology:

1. The underlying physical system is stochastic.
2. The signal is the output of a deterministic but high-dimensional system, with a dimension too high to be extracted from the given time series of finite length.
3. The signal represents a system to which noise is coupled intrinsically to the dynamics.
4. The analyzed time series is the result of different physical systems which are independently operating at the same time, e.g., different uncoupled radio burst sources simultaneously present on the sun, whose emissions sum up to the measured signal.
5. Despite the careful data selection, the measurement noise is still too high for the kind of analysis carried out and dominates the results.
6. The choice of the time delay τ, which is a quite critical and sensitive parameter in the correlation dimension analysis, is not optimal.

4.1.2. No scaling region

There exist cases, in which for increasing embedding dimension m the scaling region disappears. In the curves of the correlation integral $C(r)$ no linear range can be detected and, correspondingly, in the graphs of the local slopes $\nu(r)$ no plateau region exists. In such cases the quantity $D_c(m)$ is not defined. An example is shown in Fig. 6. The main reason for such a behavior might be that the analyzed data set is too short and/or too strongly contaminated by noise. In such a case the deviations from ideal scaling at small and large length scales r merge at intermediate r, and cause the scaling region to disappear. This effect is stronger for higher embedding dimensions, since for increasing m the attractor is sparsely covered with points, which can be verified in Fig. 6. As shown by Schreiber & Kantz (1995), even small amounts of measurement noise can conceal possible scaling behavior.

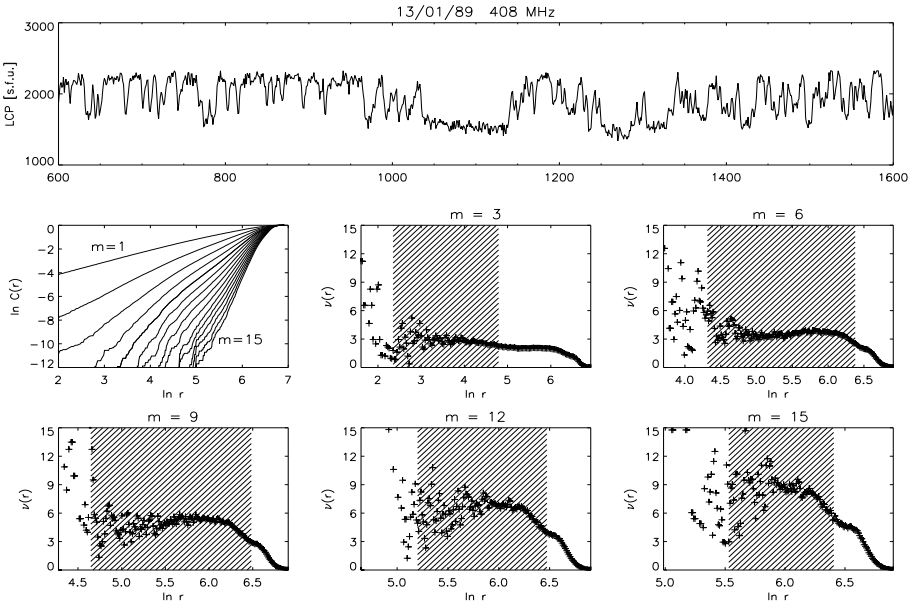

Fig. 5. Top panel: Stationary subsection of a type IV event with sudden reductions (January 13, 1989). The left panel of the middle column shows the correlation integral $C(r)$ for $m = 1$ to $m = 15$. The graphs of the local slopes $\nu(r)$, plotted for $m = 3$, 6, 9, 12 and 15, reveal distinct plateau regions (hatched), which for increasing m are moving to higher values, indicating that the $D_c(m)$ are divergent.

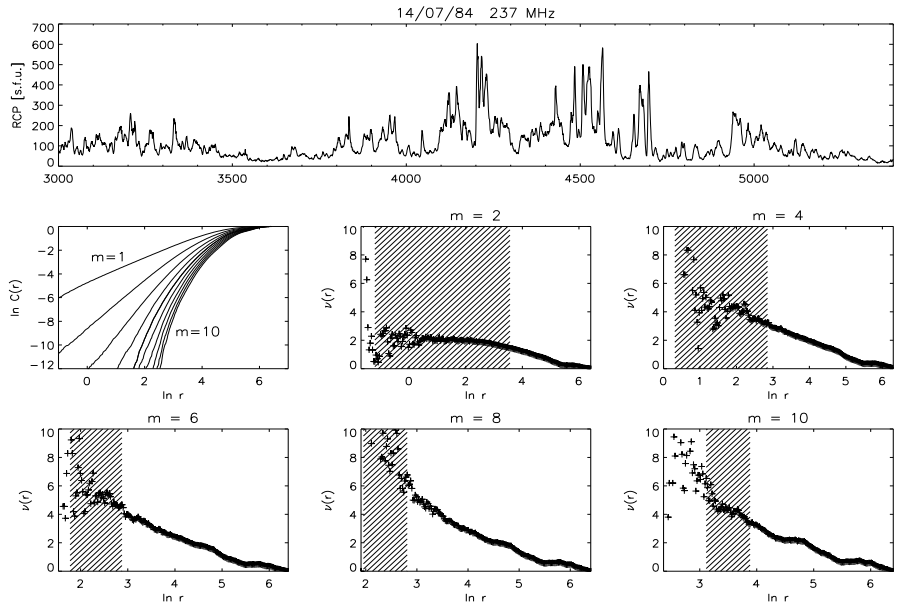

Fig. 6. Top panel: Stationary subsection of a type IV event (July 14, 1984). The curves of the correlation integral $C(r)$, plotted for $m = 1$ to $m = 10$, reveal only for small m a linear range. In the graphs of the local slopes $\nu(r)$, the plateau region (hatched) shrinks with increasing m, and for $m \gtrsim 6$ no distinct scaling region exists.

4.1.3. Deformed scaling region

The third case, in which the correlation dimension analysis led to negative results, is, that the curves of the correlation integral are highly deformed. Such deviations from ideal scaling are mainly caused by the presence of intermittent sections, or generally, by the presence of very different amplitude scales in the data. Fig. 3 shows such deformed scaling regions for a stationary subsection of a sample type I storm, caused by an intermittent section. This can be clarified as the elimination of the intermittent section causes the deformation to disappear. Explained by the typical presence of intermittent phases in type I storms, the correlation dimension analysis rather often results in deformed plateau regions for type I burst series.

4.2. Local pointwise dimension analysis

The third set of columns in Table 1 and Table 2 contains the results of the pointwise dimension analysis for the type I and the type IV events, respectively. $\bar{D}_p$ gives the averaged pointwise dimension with standard deviation σ, calculated over an embedding range $m = 10 - 13$, and "ok" denotes the percentage of points which passed the scaling and convergence test. $\Delta\bar{D}_p$ gives the increase of the averaged pointwise dimension, when the embedding range is increased by two dimensions, from $m = 10-13$ to $m = 12-15$. "surr." denotes the outcome of the surrogate data test, and positive means that the null hypothesis, which states that the results are caused by linearly corre-

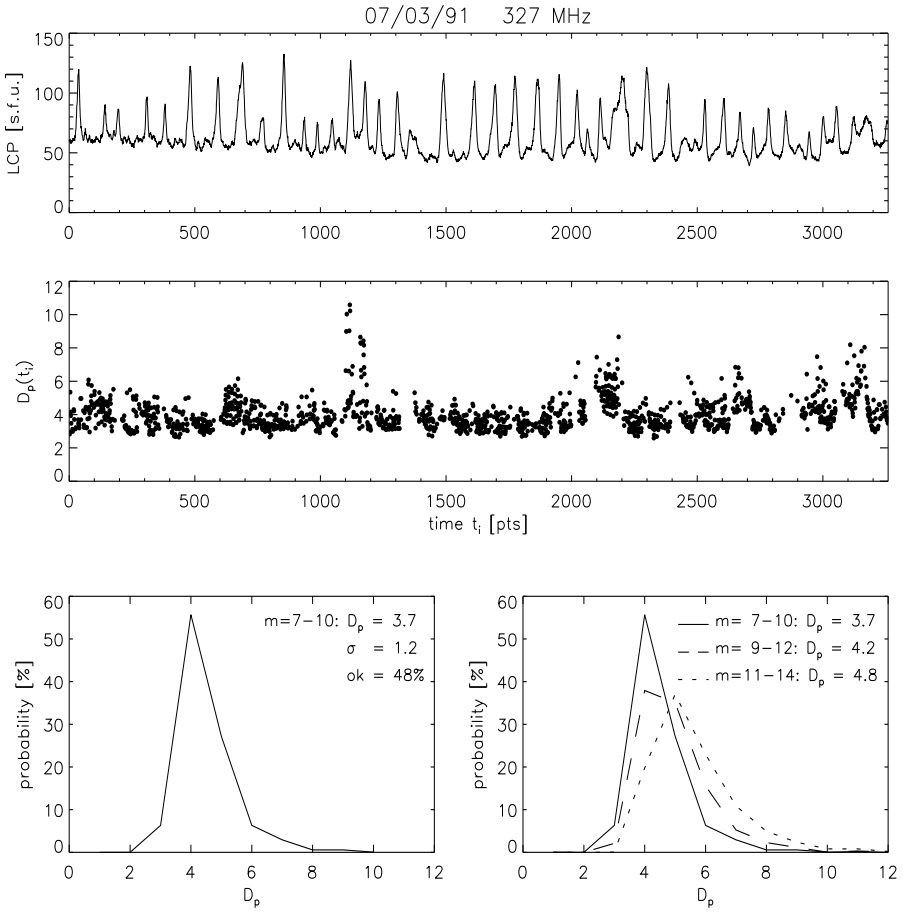

Fig. 7. The top panel depicts the time series of a type IV event with pulsations (March 7, 1991). The middle panel shows the evolution of the local pointwise dimensions. The left bottom panel shows the histogram of the dimension values. In the right botton panel we show the same histogram, overplotted by the histograms of dimensions calculated at higher embedding ranges.

lated noise, can be rejected, and that significant evidence for nonlinearity in the data is given.

As an example, Fig. 7 illustrates the results of the local pointwise dimension analysis obtained for a type IV event with quasi-periodic pulsations. The top panel shows the time series, the middle panel the time evolution of the local pointwise dimensions, $D_p(t_i)$. In the bottom panels the histograms of the local dimensions are plotted, calculated over different embedding ranges. About half of the points of the time series passed the scaling and convergence test and were used to compute the averaged pointwise dimension. However, as the histograms of the local dimensions calculated over increasing embedding dimensions ($m = 7-10$, $m = 9-12$, $m = 11-14$) reveal, no absolute convergence exists, but a slight increase with increasing m-ranges occurs. This can be clearly seen in the right bottom panel of Fig. 7, as for higher embedding ranges the center of the histogram moves to higher dimension values. The same phenomenon occurs for all analyzed samples, as the positive $\Delta\bar{D}_p$ values indicate, on the average $\Delta\bar{D}_p \approx 5\%$.

This phenomenon, on the one hand, could result from the fact that the $D_p(\boldsymbol{\xi}_i)$ do not really converge with increasing m and no convergence to a low-dimensional attractor exists. On the other hand, a comparison with simulated time series from well known chaotic attractors contaminated with Gaussian noise reveals a similar behavior. For selected samples we repeated the analysis after application of a simple nonlinear noise reduction to the data

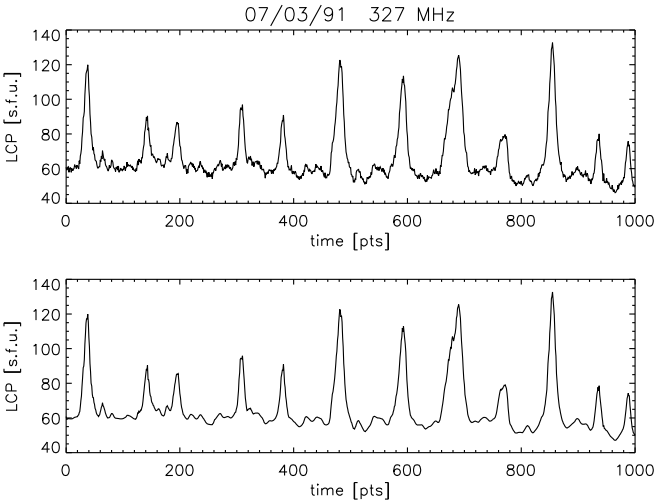

Fig. 8. Illustration of the application of a nonlinear noise reduction. The top panel shows the original time series (subsection of a type IV with pulsations, March 7, 1991). The bottom panel shows the same series after the application of the noise reduction.

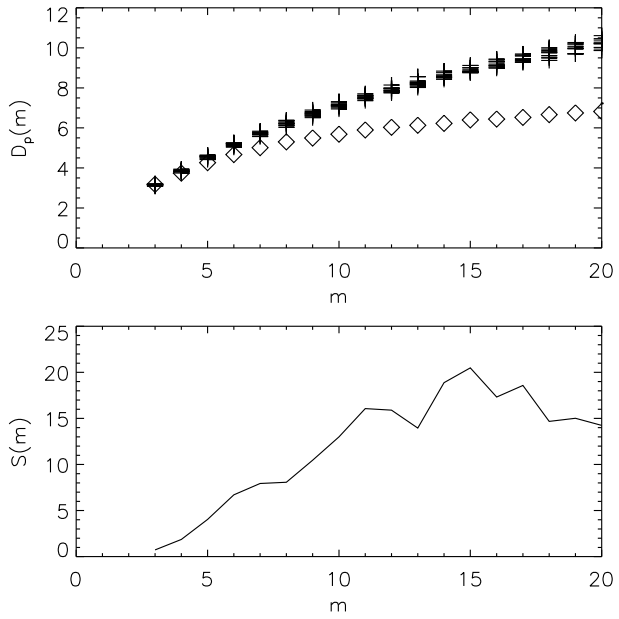

Fig. 9. Illustration of the outcome of the surrogate data test for a type I storm (January 30, 1991). The top panel shows the averaged pointwise dimensions, calculated for the original data (diamonds) and for an ensemble of 10 surrogates (crosses), for $m = 3$ to $m = 20$. In the bottom panel the significance S is plotted, which reaches values significantly larger than the 3σ level, giving evidence on nonlinearity in the data.

(Schreiber 1993), to find out if the increase is caused by measurement noise. As it is common in nonlinear time series analysis, the used noise reduction method does not rely on frequency information but makes use of the structure in the reconstructed phase space. Fig. 8 shows an example of the application of the noise reduction method. Repeating the analysis with the times series after the application of the noise reduction led to the effect, that the dimension increase is softened but not fully eliminated though. Such result suggests that the dimension increase is not caused by measurement noise contaminating the signal of a deterministic system.

The surrogate data analysis yields a positive outcome for most of the analyzed samples, indicating that the obtained results are not an artifact, which could arise when the analysis is applied to non-stationary stochastic data. For $\approx 75\%$ of the type I and $\approx 85\%$ of the type IV burst time series with a significance of 3σ, we can reject the null hypothesis that the results are caused by a linear stochastic process, and have evidence for nonlinearity in the data. Fig. 9 illustrates the outcome of the surrogate data analysis for a sample type I storm. The top panel shows the averaged pointwise dimension as a function of the embedding dimension m, calculated from all points passing the scaling test. Diamonds represent the original data, crosses the surrogates. The bottom panel shows the related significance S, which reaches at the maximum a level of $\approx 20\sigma$, giving strong evidence for nonlinearity in the data. However, corresponding to the positive $\Delta\bar{D}_p$ values, the $\bar{D}_p(m)$ of the original data slightly increase with increasing m and do not show a definitive convergence to a finite dimension value.

5. Discussion

The outcome of the dimension analysis does not allow to claim low-dimensional determinism for the analyzed data sets. First, the correlation dimension analysis failed in all cases. Second, the obtained averaged pointwise dimension values $\bar{D}_p$ are too high to characterize a low-dimensional physical system. Third, the $\bar{D}_p$ do not reveal an absolute convergence with increasing embedding dimension m. On the other hand though, the local pointwise dimensions obtained over a specific embedding range yield a quite distinct behavior, and the surrogate data analysis evidences nonlinearity in the data.

In Fig. 10 we show a comparison of the correlation dimension and the local pointwise dimension analysis of a sample type IV event. The correlation integral and the related local slopes do not give any evidence for low-dimensional determinism, since no significant scaling region and no convergent behavior occurs. However, the corresponding curves of the local pointwise dimension analysis reveal a distinct scaling region and a clear convergence to a finite and low dimension value for certain points $\boldsymbol{\xi}_i$. The figure clearly illustrates that the calculated local dimensions do not represent an artifact, which might arise, for instance, if the automatic scaling and convergence procedure is not well adapted to the analysis. Moreover, such comparison suggests that the local dimension analysis of a times series is more robust than the classical correlation dimension method. The main reason might be that in the correlation dimension analysis the scaling behavior itself is a global property, since *all* pairs of points contribute to the correlation integral, and the scaling region can possibly be smeared out by such an averaging process. Contrary to that, the local pointwise dimensions are based on the scaling behavior at *each* single point, and can reveal a well defined scaling at certain points.

In Table 3 we give a summary of the averaged pointwise dimensions for the different event types. For the type IV events we additionally calculated the quantities separately for the different subtypes. We list the event type, the number of events belonging to each type (or subtype), the number of events passing the surrogate test, and the average of the pointwise dimensions over the respective event types, calculated only from the samples for which the surrogate data test gave a positive result. On the average, the type I storms reveal lower $\bar{D}_p$ values than the type IV events and a significant smaller standard deviation, indicating that type I storms represent a compar-

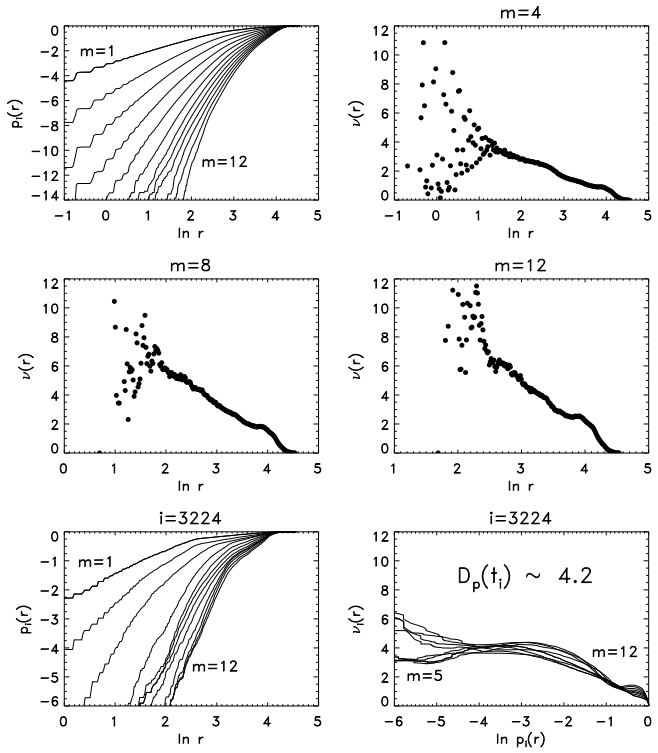

Fig. 10. Comparison of the correlation dimension and the local pointwise dimension analysis, calculated for a type IV burst series with pulsations (March 7, 1991). The top and middle panels illustrate the correlation dimension analysis. The left top panel shows the curves of the correlation integral $C(r)$ for embedding dimensions $m = 1$ to $m = 12$. The top panel at the right hand side and the middle panels depict the curves of the local slopes $\nu(r)$ for three different embedding dimensions. The bottom panels illustrate the outcome of the local pointwise dimension analysis for point $i = 3224$. The left bottom panel shows the curves of the probability $p_i(r)$. In the right bottom panel we show the curves of the related local slopes $\nu_i(r)$.

Table 3. Statistics of the pointwise dimensions. We list the number of events belonging to a particular type or subtype (including type IV events with fine structures of no particular kind, pulsations, fast pulsations, sudden reductions, and spikes), the number of events giving a positive outcome of the surrogate data test, and the pointwise dimension averaged over the respective (sub)type.

type	number	surr. pos.	$\bar{D}_p^{type}$
type I storms	30	23	5.4 ± 0.4
type IV events	27	23	6.4 ± 1.0
type IV fine str.	7	6	5.9 ± 0.4
type IV puls.	6	5	5.5 ± 0.7
type IV fast puls.	7	5	7.4 ± 0.5
type IV sudd. red.	3	3	5.6 ± 0.4
type IV spikes	4	4	6.3 ± 0.6

atively homogeneous class. The large standard deviation for the type IV burst series basically reflects the different subtypes. The average of the particular type IV subtypes yields $\bar{D}_p$ values which are significantly different: pulsations and sudden reductions reveal the lowest values, followed by the type IVs with fine structures of no particular kind and spikes, whereas the fast pulsations are characterized by the highest values.

Such statistics suggests that the $\bar{D}_p$ are quite well representing the different types of radio bursts under investigation. This means that even if low-dimensional determinism cannot be proved, the local dimension analysis can provide a quantitative description of the events, which is not possible with the commonly used correlation dimension. As argued by Schreiber (1999), such description has the drawback that it does not provide an invariant characterization of a system. On the other hand, it offers an alternative statistical approach for systems, for which pure determinism cannot be established. This is of particular interest in astrophysics, since astrophysical systems represent real-world systems, which cannot be influenced by the observer and are highly interconnected with their surroundings, making pure determinism rather improbable.

Moreover, we claim that on a comparative basis the retrieved dimension values are related to the degree of freedom of the system. From numerical experiments with known chaotic attractors contaminated with Gaussian noise we retrieved pointwise dimensions, which are slowly increasing with increasing embedding dimension m, i.e. the absolute convergence to the definite attractor dimension disappeared due to the contamination of the deterministic signal with a stochastic component. This behavior is similar to the one of the analyzed radio events. However, from this similarity we cannot conclude that the pointwise dimension analysis is indicative for hidden deterministic chaos in the radio burst time series, since the retrieved dimension values are too high to characterize low-dimensional determinism, and for a reliable dimension analysis of high-dimensional systems much longer time series are needed than we have at disposal (– a limitation which is intrinsic to time series representing real-world systems). Nevertheless, what we can infer from this similarity is that the retrieved dimension values, even if not representing attractor dimensions, are still indicative for the degree of freedom of the physical system underlying the time series, characterizing its complexity. Based on this fact, we make use of the retrieved dimension values to describe the complexity of the related systems in a comparative way, without claiming or supposing the presence of low-dimensional determinism.

6. Conclusions

In the following items we give a summary of the main results obtained by the presented dimension analysis of several types of solar radio events, based on the correlation

dimension and the local pointwise dimension method. The results are relevant concerning the physics of the analyzed events as well as the different methods applied.

1. The analysis does not enable to claim low-dimensional determinism in the time series. This outcome is in agreement with the results obtained by Isliker (1992b) and Isliker & Benz (1994a, 1994b), who also, among others, investigated type I storms, type IV events, and spikes. We cannot confirm the results of Kurths & Herzel (1986, 1987), Kurths & Karlický (1989), and Kurths et al. (1991), who obtained finite dimension values for decimetric pulsations. However, the outcome of the present paper does not exclude deterministic chaos in the analyzed time series but makes pure low-dimensional determinism, characterized by few free parameters, rather improbable.
2. The analyzed time series are not fully stochastic, i.e. white noise. This fact we infer from the distinctly slower increase of the dimension values with increasing embedding dimension than expected for fully stochastic processes, which always fill the whole phase space, i.e. $D(m) \approx m$. Moreover, the surrogate data analysis suggests that the time series do not represent linear stochastic processes.
3. For most of the analyzed data sets we have evidence that nonlinearity in the time series is present (given on a 3σ level by means of a surrogate data test).
4. A comparison of the two different methods used for the determination of fractal dimensions reveals that the local dimension method is more stable and enables more physical insight than the classical correlation dimension method. The local dimension analysis can provide a statistically significant quantity for systems, which cannot be characterized by invariants of the dynamics, probably since they are in fact not purely deterministic. Such quantities can be of special interest for comparative studies, investigating interrelations between different time series (which, e.g., can be useful for classificational purposes) or investigating intrarelations in between one time series (in order to detect dynamical changes).
5. The retrieved pointwise dimension values can be interpreted in terms of complexity of the underlying physical system. In this frame our analysis indicates that spikes and fast pulsations are the signature of systems of higher complexity than pulsations, sudden reductions and type I storms.

In relation with other kind of analysis of solar radio bursts the presented results might give further ideas on the physics of the events. In the following we present a short discussion in this respect, applied to pulsation and spike events, which are quite striking features associated with solar flares.

Spikes have been intensively studied during recent times. Their short duration and small bandwidth gives rise to the evidence that they are associated with the energy fragmentation process in solar flares (Benz 1985, 1986). Based on this connection, Schwarz et al. (1993) performed a nonlinear analysis by means of symbolic dynamics methods, interpreting the spikes appearance in the frequency-time domain as spatio-temporal patterns. This analysis gives indications that the simultaneous appearance of spikes at different frequencies is not a purely stochastic phenomenon but may be caused by a nonlinear deterministic (not necessarily low-dimensional) system or by a Markov process, compatible with a scenario in which spikes at nearby locations are simultaneously triggered by a common exciter, i.e. the localized sources are causally connected. In the present paper we find evidence for the spike events analyzed, that they do not represent a purely stochastic phenomenon in their temporal order either, even if the degree of freedom of the related physical system is expected to be quite high. Interpreting this result in the frame of the scenario suggested by Schwarz et al. (1993), it might give indications that the triggering of successive spikes by a localized source is not caused by a fully stochastic process, but reveals some (possibly weak) kind of nonlinear causal connection. However, this inference is restricted to the assumption that the spikes time series rather reflect the physical conditions of the triggering mechanism than those of the emission.

Pulsations, although a rather marginal phenomenon in the course of solar flares, have reached a wealth of attention, especially due to the very regular features they sometimes reveal (for a review see Aschwanden 1987). In previous investigations of the dimensionality of solar pulsations (Kurths & Herzel 1986, 1987; Kurths & Karlický 1989; Kurths et al. 1991) the presence of low-dimensional determinism is reported, with dimensions $2.5 \lesssim D \lesssim 3.5$. Moreover, for one single event a dynamical evolution from a limit cycle to a low-dimensional chaotic behavior was found (Kurths & Karlický 1989). Although we cannot confirm these results, we want to stress that our analysis suggests that pulsation events, especially quasi-periodic pulsations, represent the least complex phenomena among the analyzed types of radio events, i.e. their degree of freedom is expected to be lower than that of other burst types, even if not low-dimensional. The inferred high-dimensionality and the nonlinear structures detected do not match with linear MHD oscillation models for pulsations (e.g., Rosenberg 1970; Roberts et al. 1984), in which only a few eigenmodes are excited, but rather favor models of self-organizing systems of plasma instabilities, which comprise periodic as well as low- and high-dimensional chaotic behavior. Such a self-organizing model for the electron-cyclotron maser instability, based on a Lotka-Volterra type equation system, is discussed in Aschwanden & Benz (1988), however restricted to limit cycle solutions.

Acknowledgements. We thank P. Zlobec for helpful discussions and his support in the data classification. A.V. and A.H. ac-

knowledge the Austrian Ministry of Sciences. M.M. acknowledges the financial support by ASI and MURST.

References

Abarbanel, H.D.I., 1996, Analysis of Observed Chaotic Data, Springer, New York
Aschwanden, M.J., 1987, Solar Phys. 111, 113
Aschwanden, M.J.., Benz, A.O., 1988, Astrophys. J. 332, 466
Benz, A.O., 1985, Solar Phys. 96, 357
Benz, A.O., 1986, Solar Phys. 104, 99
Brandstater, A., Swinney, H.L., 1987, Phys. Rev. A 35, 2207
Casdagli, M., Eubank, S., (eds.), 1992, Nonlinear Modeling and Forecasting, Sante Fe Institutes in the Science of Complexity, Proc. vol XII, Addison-Wesley, Reading, MA
Eckmann, J.-P., Ruelle, D., 1992, Physica D 56, 185
Fraser, A.M., Swinney, H.L., 1986, Phys. Rev. A 33, 1134
Grassberger, P., Procaccia, I., 1983a, Phys. Rev. Lett. 50, 346
Grassberger, P., Procaccia, I., 1983b, Physica D 9, 189
Grassberger, P., Schreiber, T., Schaffrath, C., 1991, Int. J. of Bifurcation and Chaos 1, 521
Isliker, H., 1992a, Phys. Lett. A 169, 313
Isliker, H., 1992b, Solar Phys. 141, 325
Isliker, H., Benz, A.O., 1994a, A&A 285, 663
Isliker, H., Benz, A.O., 1994b, Space Sci. Rev. 68, 185
Isliker, H., Kurths, J., 1993, Int. J. of Bifurcation and Chaos 3, 1573
Kantz, H., Schreiber, T., 1997, Nonlinear Time Series Analysis, Cambridge University Press, Cambridge Nonlinear Science Series, vol. 7
Kugiumtzis, D., Lillekjendlie, B., Christophersen, N., 1994a, Identification and Control 15, 205
Kugiumtzis, D., Lillekjendlie, B., Christophersen, N., 1994b, Identification and Control 15, 225
Kurths, J., Herzel, H., 1986, Solar Phys. 107, 39
Kurths, J., Herzel, H., 1987, Physica D 25, 165
Kurths, J., Karlický, M., 1989, Solar Phys. 119, 399
Kurths, J., Benz, A.O., Aschwanden, M.J., 1991, A&A 248, 270
Mayer-Kress, G., 1994, Integrative Physiological and Behavioral Science 29, 203
Osborne, A.R., Provenzale, A., 1989, Physica D 35, 357
Osborne, A.R., Kirwan, A.D., Provenzale, A., Bergamasco, L., 1986, Physica D 23, 75
Roberts, B., Edwin, P.M., Benz, A.O., 1984, Astrophys. J. 279, 857
Rosenberg, H., 1970, A&A 9, 159
Schreiber, T., 1993, Phys. Rev. E 47, 2401
Schreiber, T., 1999, Phys. Rep. 308, 1
Schreiber, T., Kantz, H., 1995, Chaos 5, 143
Schwarz, U., Benz, A.O., Kurths, J., Witt, A., 1993, A&A 277, 215
Shannon, C.E., Weaver, W., 1962, The Mathematical Theory of Information, University of Illonois Press
Skinner, E., Carpeggiani, C., Landisman, C.E., Fulton, K., 1991, Circulation Research 68, 966
Takens, F.: 1981, Detecting Strange Attractors in Turbulence. In: Dynamical Sytems and Turbulence, Rand D.A., Young L.S. (eds.), Lecture Notes in Mathematics, vol. 898, Springer, New York, 366
Theiler, J., 1986, Phys. Rev. A 34, 2427
Theiler, J., Eubank, S., Longtin, A., Galdrikian B., Farmer, J.D., 1992, Physica D 58, 77
Weigend, A.S., Gershenfeld, N.A., (eds.), 1993, Time Series Prediction: Forecasting the Future and Understanding the Past, Sante Fe Institutes in the Science of Complexity, Proc. vol. XV, Addison-Wesley, Reading, MA